

Band gaps and stability of CsSiX₃ halides.

Santosh Kumar Radha and Walter R. L. Lambrecht

Department of Physics, Case Western Reserve University, 10900 Euclid Avenue, Cleveland, OH 44106-7079, USA

Key words: halides, Si-based, band structure, metastability

* Corresponding author: e-mail walter.lambrecht@case.edu

There is a great current interest in lead-free halide perovskites. While Sn based and Ge based compounds of this type have already been demonstrated experimentally, Si based ones have not. In this paper, we consider the possibility of CsSiX₃ halide perovskites. While previous work for cubic CsSiI₃ found the band gap to close or in fact become inverted and to lead to a topological insulator, we show here that in the rhombohedrally distorted structure that occurs because of Si off-centering, the band gap becomes larger than 1.5 eV and possibly of interest for photovoltaics. On the other hand, even in the cubic structure at high temperature, fluctuations of the Si position, would lead to a sizable gap. The total energy calculations, show that the materials are unstable toward $3\text{CsSiI}_3 \rightarrow \text{Si}_2\text{I}_6 + 3\text{CsI} + \text{Si}$ and $2\text{CsSiI}_3 \rightarrow \text{SiI}_4 + 2\text{CsI} + \text{Si}$ and are thus above the convex hull. Similar results are presented for halogens: I, Br, Cl.

Copyright line will be provided by the publisher

1 Introduction The hybrid organic/inorganic as well as the all inorganic halide perovskites such as (MA)PbX₃, with MA = methylammonium = CH₃NH₃, CsPbX₃, SnSnX₃, with X=I, Br and Cl, have recently drawn significant attention as opto-electronic materials, primarily for photovoltaics but also for light-emitting diodes, and non-linear optics [1–8]. The key to these properties lies in the perovskite structure, which consists of corner-sharing octahedra and the corresponding band-structure for ABX₃ with B a group-IV element, X a halogen and nA a large alkali ion. The rather deep *s*-electrons of the group IV-elements Sn and Pb, leads to a valence band maximum (VBM) at the corner of the simple cubic Brillouin zone consisting of antibonding IV-*s* with X-*p* states. The conduction band minimum (CBM) at the same point consists of IV-*p* states, which are by symmetry not interacting with either X-*p* or *s* orbitals at that point in the Brillouin zone [9]. This leads to optical transitions that are direct in *k*-space as well as in some sense in real space since the *s* → *p* transitions are allowed on the same group-IV atom in the centrum of the octahedron. The antibonding nature of the VBM and related band dispersion also leads to low hole mass and in the case of Pb or Sn, the strong spin-orbit coupling in the *p* state derived CBM leads also to a small electron mass, both beneficial for transport.

An important problem is the stability of these materials with respect to alternative crystal structures. A second problem is that Pb is undesirable in these materials from the environmental point of view. From this point of view it is of interest to consider other IV-elements, Sn, Ge and Si. Other group-II elements as B ion in ABX₃ could also be considered but typically lead to a different type of indirect band structure. Regarding the stability, the ideal cubic perovskite is found to be unstable with respect to soft phonons[10]. In a recent paper[11] we showed that the Sn and Pb based perovskites' primary distortion mode is through octahedron rotation. This leads to a tetragonal phase, and eventually after rotation about two orthogonal axes an orthorhombic phase [10]. In addition, there exist another orthorhombic phase, in which octahedra share edges, known as the "yellow phase". While the rotations maintain roughly the same band structure with a slight increase in gap, the yellow phase has a much higher band gap [9] and loses the attractive band structure features for the intended applications. On the other hand, Ge and Si based perovskites were found to distort differently [11]. Namely, they undergo an off-centering of the Ge or Si along the cubic body diagonal, which is then coupled to a rhombohedral distortion [12]. It was shown that this results from the strong lone-pair character of Ge or Si when forced to be divalent. In fact, it also occurs for Sn and Pb under expansion

Copyright line will be provided by the publisher

of the lattice constant, but does not lead to a separate rhombohedral phase because these off-centring distortions only occur at high temperature and are then merely local fluctuations about the average cubic phase [13]. For Ge based halide compounds, another monoclinic phase needs to be considered, in particular for smaller A-cations like Rb [12]. The relative stability of the rhombohedral and monoclinic forms will be discussed elsewhere. The Goldschmidt tolerance factor which is slightly larger than 1 for the Si and Ge based perovskites[14] does not prevent the formation of a perovskite but is an indicator that it will not be subject to octahedral rotation type distortions.

Here we focus on the properties of the Si-based rhombohedral and cubic perovskite phases. The Si-based perovskites were first considered in Ref. [14]. It was found there that the gap in the family of cubic perovskite CsBI_3 decreases with B from Pb down the column of group IV to Si and by the time we reach Si, the gap becomes inverted and would lead to a topological insulator if that phase exists. In that paper, we found that the cubic perovskite phase was probably unstable or at best marginally stable. In particular, one might think that the stronger tendency of Si to allow only a tetravalent state, could inhibit the formation of the perovskite crystal structure. Here we further investigate the potential stability or metastability of CsSiX_3 in the distorted rhombohedral structure and secondly calculate their band structures. We also reconsider the problem of the band gap of the cubic phase from the point of view that this would be a high-temperature phase in which fluctuations of the Si atom about its central position in the octahedron can still be expected. In that case, the gap must be estimated as an thermodynamic average over these fluctuating structures rather than simply evaluated at the average position of the Si.

2 Computational Methods Our calculations of the energetic stability use the density functional theory in the generalized gradient approximation for exchange and correlation [15]. The self-consistent charge density, relaxed structures, total energies and band structures are calculated using the all-electron full-potential linearized muffin-tin orbital method (FP-LMTO)[16,17] as implemented in the *questaal* package[18]. The band structures are calculated using a many-body perturbation theory approach: the quasi-particle self-consistent (QS) *GW* method where G and W are the one-electron Green's function and screened Coulomb interaction W respectively. In the *QSGW* approach, the energy dependent self-energy $\Sigma(\omega) = iGW$ is replaced by a hermitean energy averaged non-local exchange correlation self-energy matrix which is iterated to self-consistency. This means that the eigenvalues or quasi-particle energies are self-consistent [19,20]. The basis set and k -point Brillouin zone integration sets are converged using a large *spdf - spd* basis set of augmented spherical smoothed Hankel functions. The k -point set used for self-consistent iterations was $12 \times 12 \times 12$ while for the *GW*

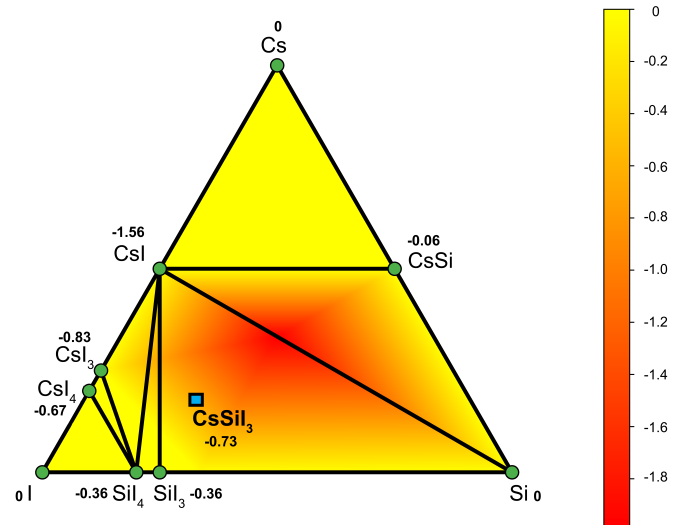


Figure 1 Ternary convex hull of the Cs-Si-I system with metastable state CsSiI_3 . The energies of formation are given with each compound on the hull, all energies in eV/atom.

calculations a $5 \times 5 \times 5$ set is used. The *QSGW* bands are interpolated by Fourier transforming from this set to real space and back to whatever k -point we wish to evaluate along the symmetry lines. The *GW* method makes the random phase approximation (RPA) for the screening of Coulomb interactions. This neglect of electron-hole interactions tends to lead to an overestimate of the band gaps which was found to amount to about 20 % in most cases [21] and is corrected by using the 0.8Σ approach in which only 80 % of the self-energy correction is applied.

3 Results

3.1 Metastability The structures were fully relaxed and the structural parameters can be found in [11] for each of the group-IV based perovskites. Here we focus on the energetic stability relative to the elements and competing binary compounds. First we check that CsSiX_3 have negative energy of formation, in other words lower energy than the sum of their elements in the standard conditions phase of room temperature and atmospheric pressure. Table 1 shows the cohesive energies of the respective elements and the energy of formation of the CsSiX_3 .

Next, we need to consider stability with respect to competing binaries. Unlike SnI_2 and PbI_2 , SiI_2 does not occur in a layered PbI_2 -type phase. Instead there exist molecular crystals based on the molecules Si_5I_{10} which has a 5-fold Si-ring, Si_2I_6 , and tetrahedral SiI_4 . The energies of formation of these phases and total energies within GGA using specific pseudopotentials are given in the Materials Project[22]. In Table 1 we compare our calculated energies of formation with those of the Materials Project for the relevant SiX_3 compound. They are found to be in ex-

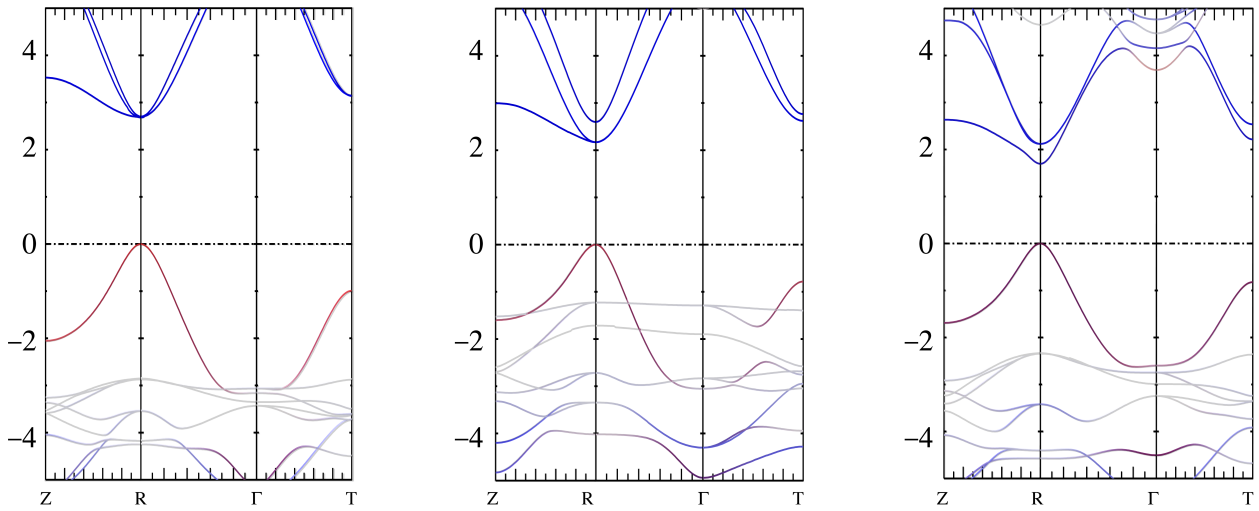


Figure 2 Band structure of the CsSiX₃ compounds in the rhombohedrally distorted perovskite structure with X=Cl, Br, I from left to right calculated in the QSGW 0.8Σ approximation. The red and blue colors indicate the amount of Si-s and Si-p orbital contributions to these bands.

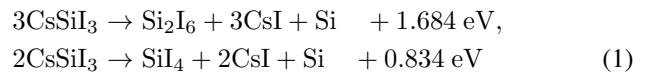
Table 1 Cohesive and Formation energies of the elements and relevant compounds in eV per atom.

Compound	E_{coh} (eV/atom) ^a	E_{form} (eV/atom)
Cs	-0.75	0
Si	-5.38	0
Cl	-1.75	0
Br	-1.58	0
I	-1.47	0
CsSiCl ₃	-3.42	-1.144
CsSiBr ₃	-3.13	-0.956
CsSiI ₃	-2.84	-0.732
SiCl ₄	-2.48	-1.721 ^b
SiBr ₄	-2.51	-0.838 ^b
SiI ₃	-2.82	(-0.379 ^a , -0.374 ^b)
SiI ₄	-2.61	-0.378 ^b
SiI ₂	-2.875	-0.306 ^b
CsCl	-2.381	-2.263 ^b
CsBr	-2.068	-1.807 ^b
CsI	-1.893	-1.566 ^b

^a Present calculation using *questaal*, ^b Materials Project, Cohesive energies calculated explicitly for the elements and the CsSiX₃. For the other cases, they are obtained from the Material Project formation energies and our cohesive energies of the elements.

cellent agreement. This allows us to place the energy of CsSiX₃ relative to the other already known compounds in the ternary system. We find that CsSiI₃ lies above the convex hull by 20 meV/atom. This is illustrated in Fig. 1. The energies of formation/atom of the compounds along the bi-

nary system lines are indicated. Specifically, we find that the reactions



are exothermic with reaction energies 112 meV/atom, 83 meV/atom respectively. It means the first reaction is the more important reaction because it is the most exothermic. The compound Si₅I₁₀ is already above the hull. Here we use the lowest energy rhombohedral relaxed structure for CsSiI₃ which is 142 meV lower than the cubic perovskite. In the case of CsSiBr₃, CsSiCl₃, only SiX₄ is on the hull, and thus only the second reaction applies. It has reaction energies of 0.184 eV/atom for the Br case and 0.622 eV/atom in the Cl case.

While these results indicate that the materials are only metastable with respect to competing binary compounds, they are not too far from the convex hull to prevent future research from trying to synthesize them. This of course does not mean that there would not be any problems with their stability. Si is well known to prefer a fourfold oxidation rather than twofold oxidation state and thus stability in air could be an issue, but evaluating this is outside the scope of first-principles calculations and would need to be determined experimentally. It is also an issue that can be prevented by suitable encapsulations as has been done in other perovskites.

3.2 Band structures of the rhombohedral phase

Although the compounds CsSiX₃ compounds were found to be only metastable, it may still be possible to synthesize them using non-equilibrium growth techniques. Here we discuss their band structures to investigate if it would be worthwhile pursuing these metastable compounds. In Fig. 2

Table 2 Band structure properties for CsSiX₃.

Compound	E_g (eV)	Δ_c (eV)
CsSiCl ₃	2.68	-0.017
CsSiBr ₃	2.16	-0.428
CsSiI ₃	1.69	0.424

we show the band structures of the CsSiX₃ compounds in the rhombohedral phase calculated in the 0.8Σ approximation. The Si-*s* and Si-*p* character of the bands is highlighted in color, so we see as usual in perovskites that the VBM has a significant Si-*s* character, while the CBM has Si-*p* character. In fact, the VBM is an antibonding state with halogen-*p* orbitals and also has a significant halogen-*p* contribution. These aspects are the same as in Sn-based and Ge-based perovskites and partial densities of states for these cases can be found in Refs. [9] and [14] respectively. We do not show them here for brevity. We can see that the gaps increase from I to Br to Cl as expected. The values of the gaps are given in Table 2. In the conduction band we may notice a sizable crystal field splitting owing to the rhombohedral distortion. Interestingly, in CsSiI₃, this leads to both the VBM and CBM being non-degenerate and having relative small masses. In CsSiBr₃ the crystal field splitting is reversed in sign with the doubly degenerate state below the non-degenerate one. This is also the case in CsSiCl₃ but the splitting in that case is smaller. We define the crystal field splitting of the CBM Δ_c to be positive if the non-degenerate a_1 symmetry state lies below the e -symmetry degenerate state of the C_{3v} group. The values of Δ_c are included in Table 2. This reversal in crystal field splitting is probably related to differences in the structural relaxation. The details of this need further study: both the rhombohedral strain and the displacement of the Si atoms, which were reported in Ref. [11] may play a role. We just note here that while in that paper we gave the displacement magnitude δu of the Si atom from its center for a given uniaxial tensile strain η along the [111] direction which minimizes the energy, we found that for CsSiI₃ the displacement is in fact, not along [111] but along $[\bar{1}\bar{1}\bar{1}]$. We plan to study the effect of the uniaxial strain on the bands and their effective masses in more detail in the near future. We note that a positive crystal field splitting also occurred for CsGeI₃, [14] but the latter has a larger band gap. A gap of about 1.7 eV and with both electron and hole masses being small and combined with the predicted ferroelectricity make CsSiI₃ a quite attractive compound for tandem photoelectric cells in combination with Si. In fact, a gap around 1.7 eV is near optimal for this application.[23–25] Spin orbit coupling is not included here because it is negligibly small.

3.3 Average band gap of the cubic phase Above a certain temperature, one expects a phase transition from the rhombohedral phase to a cubic perovskite phase. This was found experimentally in the family of CsGeX₃[12]. In

Ref. [14] we found the gap for the cubic structure of CsSiI₃ to be negligibly small and purely due to spin-orbit splitting because band inversion places the R_{15} , which in the other cases (like CsGeX₃ or CsSnX₃) is the CBM, below the R_1 , normally the VBM. There is then a forced degeneracy which is lifted by the spin-orbit coupling and hence leads to a small (20 meV only) gap. However, this approach neglects the fact that the cubic structure at high temperature is only an average structure with fluctuations of the Si atoms about the central position of the octahedron and corresponding relaxations in the lattice. It also neglects that at higher temperature the increased lattice constant in these materials may lead to a higher gap. To model the gap more accurately, we need a supercell and take a thermodynamic average of the gap over the various local configurations. We use a 40 atom cell and consider various random positions of the Si in their octahedra. These are taken according to the probability distribution

$$P(\vec{X}) \propto \exp(-E_{tot}(\vec{X})/k_B T) \quad (2)$$

$$\vec{X} = \{X_1, X_2, \vec{X}_3\}$$

Where:

- X_1 : is the lattice volume,
- X_2 : is the uniaxial strain η
- \vec{X}_3 : is u_i displacement vector for the 8 Si atoms

for each specific configuration X . A configuration here is determined by the global volume and uniaxial strain and the positions of the Si atoms. In the process of relaxing the CsSiI₃ structure, we assembled a data base of different Si positions, lattice constants and strains η for the 5 atom cell. Interpolating between these we obtain the $E_{tot}(X)$ in the multidimensional space and can convert this into a Boltzmann distribution function and pick random structures with probability according to this distribution, where for each global a and η we pick the 8 Si positions according to the corresponding distribution. The band gaps of these random 40-atom cells are averaged according to

$$\langle E_g \rangle = \sum_n P(n) E_g(n) \quad (3)$$

with n sampled from the normalized distribution function. In Fig. 3 we show an example random structure. In Fig. 4 we show the specific gaps of these random structures. We also show their range and average value. These band gaps are LDA band gaps. The QSGW gap correction is about 1 eV and can be assumed to stay constant between the rhombohedral and cubic structures. We find that the average gap is slightly lower than the value of the low temperature equilibrium rhombohedral structure but clearly much higher than zero, as the gap at the average cubic structure would have given. It turns out that the spread in different

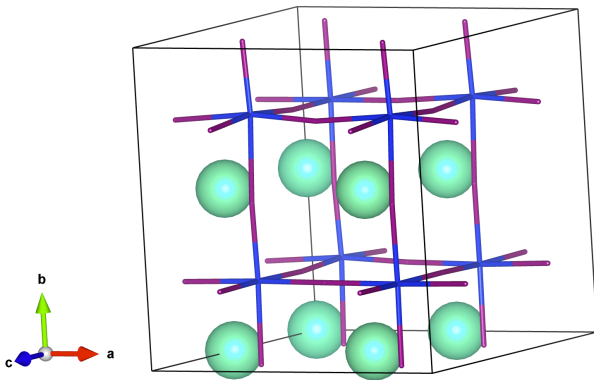


Figure 3 One of the quasi-random structures used to compute the band gap chosen with probability given by Eq.(2)

values here occurs mostly because of the different Si positions, but the average difference in energy from the perfect cubic zero gap is mostly because we have a larger lattice constant. This is because the rhombohedral structure has a larger optimum value than the cubic structure. The rhombohedral distortion expands the volume as we found in Ref. [11]. The local rhombohedral distortions are driven by the Si displacements and hence lead to a larger lattice constant even in our average cubic structure if we assume it can be modeled by the above distribution function. Thus while we did not use explicitly a temperature dependent lattice constant we ended up with a larger lattice constant closer to that of the optimized rhombohedral structure in the course of our averaging procedure. Obviously, at present we have no information on the thermal expansion coefficient or the existence of a cubic phase, since the material has not yet been synthesized. Thus one should interpret this result as giving only a qualitative indication that the gap of the cubic phase will be close to that of the rhombohedral phase rather than close to zero as a perfect cubic structure would have given.

4 Conclusions In this paper we have evaluated the thermodynamic stability of CsSiX_3 perovskite structure crystals. We find the rhombohedrally distorted structure $R\bar{3}m$ with off-centered Si position to have negative energies of formation but to lie slightly above the convex hull with respect to SiX_4 and in the case of iodine, Si_2I_6 structures. Nonetheless, they may be possible as metastable compounds. They are found to have band gaps in the useful range of 1.69 to 2.68 eV. In particular CsSiI_3 is found to have a band gap suitable for single material or tandem solar cells and also has quite small effective masses for both holes and electrons. The Br and Cl materials have somewhat higher gaps but may still be useful because of the unusually small hole masses. The ferroelectric distortion of these materials which lacks an inversion symmetry may also imbue them with useful nonlinear optical properties, such as the shift current. Further work to evaluate these properties as well as a detailed description of the effective masses

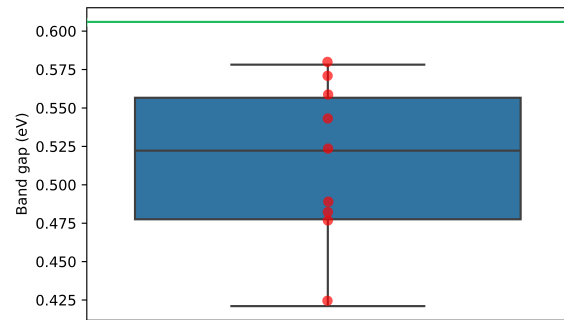


Figure 4 LDA band gaps of the quasi-random structures (red dots), their average (solid black line) and range (blue region indicates the 1σ region, short black lines indicate maximum and minimum), and band the gap of the corresponding fully relaxed rhombohedral CsSiI_3 (green line)

and the dependence of the crystal field splitting on strain is needed.

Acknowledgements This work was supported by the U.S. Department of Energy, Basic Energy Sciences under grant number DESC0008933. The calculations made use of the High Performance Computing Resource in the Core Facility for Advanced Research Computing at Case Western Reserve University.

References

- [1] A. Kojima, K. Teshima, Y. Shirai, and T. Miyasaka, *Journal of the American Chemical Society* **131**(17), 6050–6051 (2009), PMID: 19366264.
- [2] M. M. Lee, J. Teuscher, T. Miyasaka, T. N. Murakami, and H. J. Snaith, *Science* **338**, 643 (2012).
- [3] J. M. Ball, M. M. Lee, A. Hey, and H. J. Snaith, *Energy Environ. Sci.* **6**, 1739 (2013).
- [4] G. E. Eperon, V. M. Burlakov, P. Docampo, A. Goriely, and H. J. Snaith, *Advanced Functional Materials* **24**, 151 (2014).
- [5] M. Liu, M. B. Johnston, and H. J. Snaith, *Nature* **501**, 395 (2013).
- [6] J. Burschka, N. Pellet, S. J. Moon, R. Humphry-Baker, P. Gao, M. K. Nazeeruddin, and M. Grätzel, *Nature* **499**, 316 (2013).
- [7] H. S. Kim, S. H. Im, and N. G. Park, *The Journal of Physical Chemistry C* **118**(11), 5615–5625 (2014).
- [8] N. G. Park, *Materials Today* **18**(2), 65 – 72 (2015).
- [9] L. y. Huang and W. R. L. Lambrecht, *Phys. Rev. B* **88**, 165203 (2013).
- [10] L. y. Huang and W. R. L. Lambrecht, *Phys. Rev. B* **90**, 195201 (2014).
- [11] S. Kumar Radha, C. Bhandari, and W. R. L. Lambrecht, *Phys. Rev. Materials* **2**(Jun), 063605 (2018).
- [12] G. Thiele, H. W. Rotter, and K. D. Schmidt, *Z. anorg. allg. Chem.* **545**, 148–156 (1987).

- [13] D.H. Fabini, G. Laurita, J.S. Bechtel, C.C. Stoumpos, H.A. Evans, A.G. Kontos, Y.S. Raptis, P. Falaras, A. Van der Ven, M.G. Kanatzidis, and R. Seshadri, *Journal of the American Chemical Society* **138**(36), 11820–11832 (2016), PMID: 27583813.
- [14] L.y. Huang and W.R.L. Lambrecht, *Phys. Rev. B* **93**(May), 195211 (2016).
- [15] J.P. Perdew, K. Burke, and M. Ernzerhof, *Phys. Rev. Lett.* **77**(18), 3865–3868 (1996).
- [16] M. Methfessel, M. van Schilfgaarde, and R. A. Casali, A Full-Potential LMTO Method Based on Smooth Hankel Functions, in: *Electronic Structure and Physical Properties of Solids. The Use of the LMTO Method*, edited by H. Dreyssé, , Lecture Notes in Physics, Vol. 535 (Berlin Springer Verlag, 2000), , 114.
- [17] T. Kotani and M. van Schilfgaarde, *Phys. Rev. B* **81**(12), 125117 (2010).
- [18] <http://www.questaal.org>.
- [19] M. van Schilfgaarde, T. Kotani, and S. Faleev, *Phys. Rev. Lett.* **96**(22), 226402 (2006).
- [20] T. Kotani, M. van Schilfgaarde, and S. V. Faleev, *Phys. Rev. B* **76**(16), 165106 (2007).
- [21] C. Bhandari, M. van Schilfgaarde, T. Kotani, and W.R.L. Lambrecht, *Phys. Rev. Materials* **2**(Jan), 013807 (2018).
- [22] <https://materialsproject.org/>.
- [23] W. Shockley and H. J. Queisser, *Journal of Applied Physics* **32**(3), 510–519 (1961).
- [24] S. R. Kurtz, P. Faine, and J. M. Olson, *Journal of Applied Physics* **68**(4), 1890–1895 (1990).
- [25] T. J. Coutts, J. S. Ward, D. L. Young, K. A. Emery, T. A. Gessert, and R. Noufi, *Progress in Photovoltaics: Research and Applications* **11**(6), 359–375 (2003).